Is *p*-Type Doping in TeO_2 Feasible?

Zewen Xiao(肖泽文)[1*], Chen Qiu(邱晨)[2], Su-Huai Wei(魏苏淮)[2], and Hideo Hosono(细野秀雄)[3]

[1]*Wuhan National Laboratory for Optoelectronics, Huazhong University of Science and Technology, Wuhan 430074, China*
[2]*Eastern Institute of Technology, Ningbo 315200, China*
[3]*MDX Research Center for Element Strategy, International Research Frontiers Initiative, Institute of Science Tokyo, Yokohama 226-8501, Japan*

(Received 6 December 2024; accepted manuscript online 17 December 2024)

Wide-bandgap two-dimensional (2D) β-TeO_2 has been reported as a high-mobility *p*-type transparent semiconductor [*Nat. Electron.* **4** 277 (2021)], attracting significant attention. This "breakthrough" not only challenges the conventional characterization of TeO_2 as an insulator but also conflicts with the anticipated difficulty in hole doping of TeO_2 by established chemical trends. Notably, the reported Fermi level of 0.9 eV above the valence band maximum actually suggests that the material is an insulator, contradicting the high hole density obtained by Hall effect measurement. Furthermore, the detected residual Se and the possible reduced elemental Te in the 2D β-TeO_2 samples introduces complexity, considering that elemental Se, Te, and $Te_{1-x}Se_x$ themselves are high-mobility *p*-type semiconductors. Therefore, doubts regarding the true cause of the *p*-type conductivity observed in the 2D β-TeO_2 samples arise. In this Letter, we employ density functional theory calculations to illustrate that TeO_2, whether in its bulk forms of α-, β-, or γ-TeO_2, or in the 2D β-TeO_2 nanosheets, inherently exhibits insulating properties and poses challenges in carrier doping due to its shallow conduction band minimum and deep valence band maximum. Our findings shed light on the insulating properties and doping difficulty of TeO_2, contrasting with the claimed *p*-type conductivity in the 2D β-TeO_2 samples, prompting inquiries into the true origin of the *p*-type conductivity.

DOI: 10.1088/0256-307X/42/1/016103 CSTR: 32039.14.0256-307X.42.1.016103

High-performance transparent oxide semiconductors (TOSs) are crucial for the advancement of next-generation transparent electronics, power electronics and energy-efficient displays.[1–3] The lack of high-mobility, *p*-type TOSs presents a significant challenge in designing bipolar transistors, inverter circuits, and transparent thin-film transistors (TFTs). This challenge arises from the deep and localized valence band maxima (VBMs) primarily composed of O 2*p* orbitals, hindering the generation and transport of holes.[4] To address this issue, a common strategy involves elevating and dispersing the VBM by utilizing cations with high-lying occupied d^{10} or s^2 orbitals that can effectively hybridize with O 2*p* orbitals.[5] Notably, the use of Cu(I) with the highest-lying d^{10} orbitals has facilitated the realization of Cu(I)-based *p*-type TOSs, exemplified by $CuAlO_2$.[5,6] On the other hand, cations with s^2 states conform to a specific atomic energy level sequence: Sn(II) → Pb(II) → Sb(III) → Bi(III) → Te(IV) → Po(IV).[7–9] For instance, SnO is recognized as a *p*-type semiconductor with a high-lying s-like VBM at −5.8 eV relative to the vacuum level (E_{vac}).[10] In contrast, PbO encounters challenges in hole doping due to its deeper Pb $6s^2$ states induced by relativistic effects,[7] resulting in a VBM at −6.2 eV.[11] Following this trend, it is anticipated that Sb_2O_3, Bi_2O_3, TeO_2, and PoO_2 may encounter similar obstacles in serving as *p*-type TOSs.

Interestingly, two-dimensional (2D) β-TeO_2 has recently been reported by Zavabeti *et al.*[12] as a high-mobility *p*-type TOS with a wide bandgap of 3.7 eV, a 2D hole density (p_{2D}) of 1.04×10^9 cm^{-2} and a high hole mobility of 141 cm$^2\cdot$V$^{-1}\cdot$s^{-1}. However, this "breakthrough" not only challenges the conventional perception of TeO_2 as an insulator[13] but also contradicts the anticipated difficulty in hole doping according to established chemical trends. Notably, Zavabeti *et al.*[12] observed that the Fermi level (E_F) of 2D β-TeO_2 is situated approximately 0.9 eV above the VBM [see Fig. 3(b) in Ref. [12]]. Calculation using the formula $p_{2D} = N_{v,2D}\exp[-(E_F - E_v)/k_BT]$ (where $N_{v,2D}$ represents the effective density of states in the valence band, typically around 10^{12} cm^{-2}, k_B is the Boltzmann constant, and T is the absolute temperature) suggests that with the reported E_F, the p_{2D} value at room temperature is negligible, less than 1 cm^{-2} (essentially zero). This implies insulating properties for 2D β-TeO_2, which sharply contrasts with the documented *p*-type conductivity demonstrating a p_{2D} value of 1.04×10^9 cm^{-2}.

It is noted that Zavabeti *et al.* synthesized the 2D β-TeO_2 samples by high-temperature surface oxidation of a eutectic mixture containing Te (5 wt%) and Se (95 wt%). Despite their efforts, residual Se was identified in the 2D

*Corresponding author. Email: zwxiao@hust.edu.cn
© 2025 Chinese Physical Society and IOP Publishing Ltd. All rights, including for text and data mining, AI training, and similar technologies, are reserved.

β-TeO_2 samples due to Se's lower oxophilicity relative to Te [see extended Fig. 3 in Ref. [12]]. Furthermore, the reduction of an extremely thin layer of β-TeO_2 to elemental Te remains a plausible event, because TeO_2 is known to undergo partial decomposition either spontaneously or upon heating, resulting the generation of tellurium suboxide (TeO_{2-x}, where x typically ranges from 0.7 to 0.9) and elemental Te.[14] Moreover, when subjected to an applied voltage of several volts, the intense electric field strength across the ultrathin layer can easily surpass the breakdown voltage, leading to the formation of elemental Te. Notably, elemental Se, elemental Te, and $Te_{1-x}Se_x$ alloy are all well-known high-mobility p-type semiconductors with three-dimensional (3D) hole densities (p_{3D}) on the order of $10^{14}\,cm^{-3}$ (equivalent to p_{2D} on the order of $10^{9}\,cm^{-2}$) and high hole mobilities ranging from hundreds to over a thousand $cm^2{\cdot}V^{-1}{\cdot}s^{-1}$,[15–17] comparable to those observed in the 2D β-TeO_2 samples. Based on these reanalyses, it appears that the p-type conductivity in the 2D β-TeO_2 samples is more likely attributed to residual elemental Se, reduced elemental or even $Te_{1-x}Se_x$, rather than originating from the 2D β-TeO_2 itself.

To date, the work by Zawabeti *et al.* has sparked significant confusion among the subsequent investigations in the field.[18–22] For instance, Shi *et al.* grew β-TeO_2 thin films, where the measured E_F was positioned nearly 2 eV above the VBM [Fig. 2(b) in Ref. [19]], suggesting zero hole density, yet they still classify β-TeO_2 as a p-type TOS.[19] Wang *et al.* delved into the "p-type conduction mechanism" in 2D β-TeO_2.[22] Incredibly, despite their calculated E_F falling within the mid-gap region, notably above the VBM (Figs. 3 and 7 in Ref. [22]), they still assert "superior p-type conductivity". Currently, there is a lack of reliable research demonstrating TeO_2 as a p-type TOS.

In this Letter, we employ density functional theory calculations (see the computational method in the supplementary material) to demonstrate that TeO_2, whether in the 3D bulk forms (α-, β-, or γ-TeO_2) or in the 2D β-TeO_2 nanosheets, inherently behaves as an insulator and presents significant challenges for carriers doping. The electronic structure calculations reveal that the deep Te $5s^2$ orbital is insufficient to elevate the VBM as effectively as the high-lying Cu $3d^{10}$ and Sn $5s^2$ orbitals to achieve p-type doping. Defect calculations for both 3D β-TeO_2 bulk and the 2D β-TeO_2 monolayer indicate that all intrinsic defects are deep and associated with high formation energies. Consequently, the equilibrium Fermi level remains consistently within the mid-gap region, independent of synthesis conditions, thus, the observed p-type conductivity in the 2D β-TeO_2 samples could not be intrinsic.

Before discussing the electronic structures of the TeO_2 polymorphs, we briefly review their crystal structures. The synthetic, colorless tetragonal α-TeO_2 (paratellurite) under ambient conditions was previously reported to exhibit a high-symmetry rutile-type structure (space group $P4_2/mnm$),[23] where each Te atom is coordinated by six O atoms, with a Te—O bond length of 2.30 Å, as shown in Fig. 1(a). Subsequent studies[23] revised the structure of α-TeO_2 to a distorted rutile-type with space group $P4_12_12$ and a doubled c axis, as depicted in Fig. 1(b). Despite this distortion, each Te atom remains 6-coordinated, forming a highly distorted octahedron, where the two short "quasi-equatorial" bonds, two short non-equatorial bonds, and two long non-equatorial bonds are 2.12 Å, 1.88 Å, and 2.87 Å, respectively. More often than not, the two long bonds are excluded, and Te is considered 4-coordinated. Thus, α-TeO_2 can be described as a three-dimensional network of corner-sharing TeO_4 or TeO_4E (E represents the lone pair of Te) disphenoids. At high pressures above 0.91 GPa,[24] α-TeO_2 transforms into a lower-symmetry phase (referred to as γ-TeO_2), which belongs to the orthorhombic space group $P2_12_12_1$, as illustrated in Fig. 1(c). This phase transition involves the splitting of the tetragonal a lattice parameter into the unequal a and b orthorhombic parameters, causing the splitting of O sites (denoted as O1 and O2) and resulting in varied bond lengths. The four shorter Te—O bond lengths range from 1.86 to 2.20 Å, while the two longer Te—O bond lengths are 2.69 Å and 3.20 Å, respectively. On the other hand, as illustrated in Fig. 1(d), the naturally occurring yellow mineral tellurite (β-TeO_2) crystallizes in an orthorhombic layered structure,[25,26] which crystallographically resembles brookite, the orthorhombic variant of TiO_2. Unlike the three-dimensional networks of α-TeO_2 and γ-TeO_2, in which the TeO_4 disphenoids are corner-sharing, the two-dimensional layers in β-TeO_2 consist of TeO_4 disphenoids by sharing alternately the O corners and the O—O edges. Each layer contains two types of O positions: those inside the layer (labeled O1) and those on the layer's surface (labeled O2). When β-TeO_2 consists of only one or a few layers, the so-called 2D β-TeO_2 is obtained.[12,27]

We now discuss the electronic structures of the well-recognized α-, β-, and γ-TeO_2 polymorphs, along with the hypothetical, high-symmetry rutile-type TeO_2 (r-TeO_2). The calculated bandgaps of these TeO_2 polymorphs are summarized in Table 1. The Perdew–Burke–Ernzerhof (PBE)[28] functional, known for significantly underestimating the bandgaps for oxides, slightly underestimates those of TeO_2 polymorphs. Specifically, the PBE-calculated bandgaps for α- and γ-TeO_2 are 2.79 eV and 3.06 eV, respectively, which are relatively close to their experimental values (3.48 eV[29] and 3.41 eV,[30] respectively). Conversely, the Heyd–Scuseria–Ernzerhof (HSE)[31,32] hybrid functional with a standard mixing parameter of 0.25 ($HSE^{0.25}$), overestimates these bandgaps. The $HSE^{0.25}$-calculated bandgaps for α- and γ-TeO_2 are 3.89 eV and 4.21 eV, notably higher than experimental values. Similarly, for β-TeO_2, which is yellow, the $HSE^{0.25}$ predicts a bandgap approximately 3.3 eV, inconsistent with its observed color. To gain more accurate bandgaps for TeO_2 polymorphs, the HSE functional with a reduced mixing parameter of 0.10 ($HSE^{0.10}$) was examined. The $HSE^{0.10}$-calculated bandgaps for α- and γ-TeO_2 are 3.21 eV and 3.51 eV, closely aligning with experimental values, while the $HSE^{0.10}$ bandgap for β-TeO_2 is 2.63 eV, consistent with its yellow appearance.[25,26] Hence, the subsequent discussion on the electronic structures and dopability of TeO_2 polymorphs will be based on $HSE^{0.10}$ results.

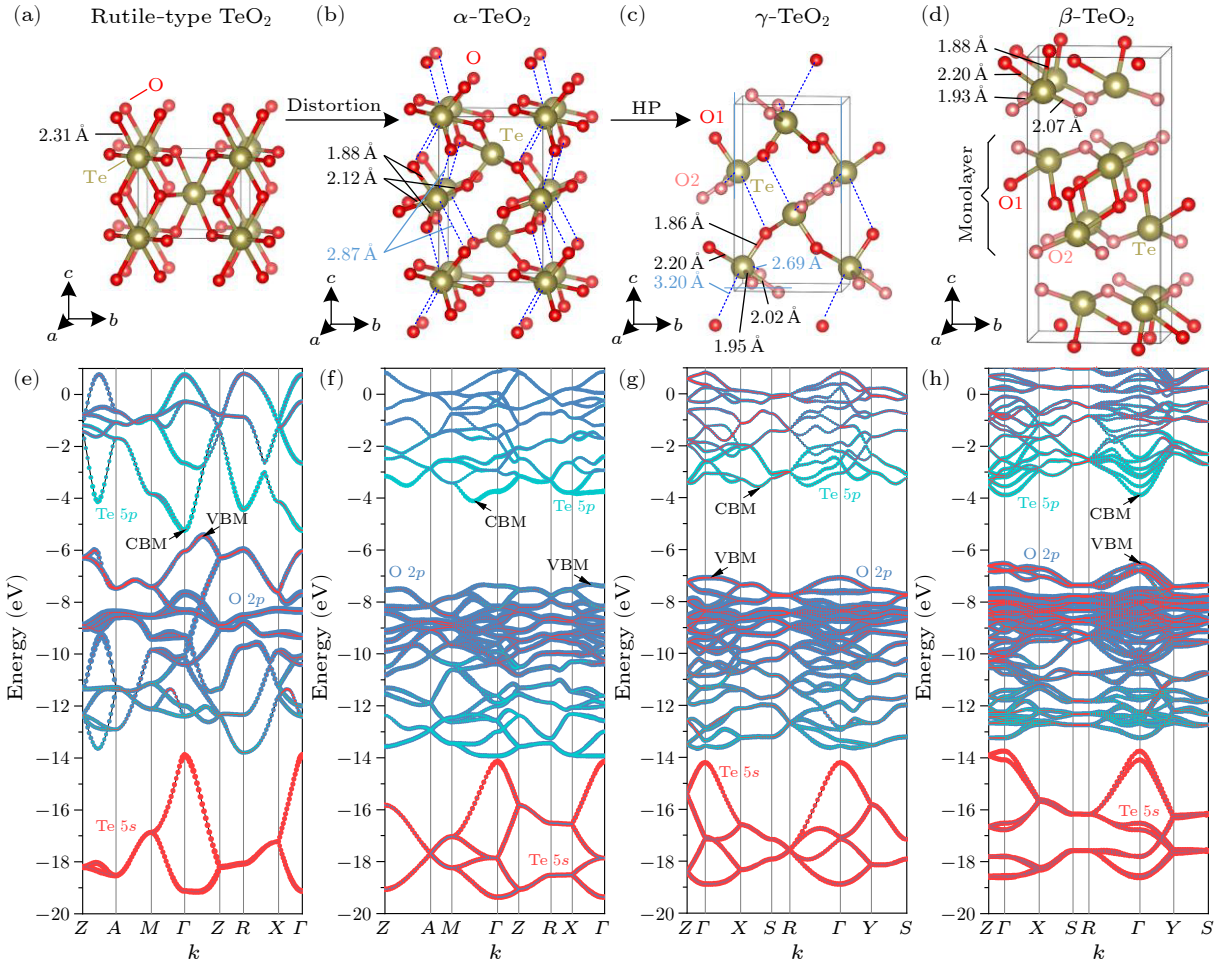

Fig. 1. (a)–(d) Crystal structures and (e)–(g) band structures calculated with the $HSE^{0.10}$ functional for TeO_2 polymorphs: (a), (e) hypothetical rutile-type TeO_2 (space group $P4_2/mnm$), (b), (f) paratellurite α-TeO_2 (space group $P4_12_12$), (c), (g) γ-TeO_2 (space group $P2_12_12_1$) and (d), (h) tellurite β-TeO_2 (space group $Pbca$). The energies are with respect the E_{vac}. The relatively deep Te $5s^2$ orbital shows limited hybridization with O $2p$ orbitals, thus impeding the elevation of the VBM as effectively as the high-lying Cu $3d^{10}$ and Sn $5s^2$ orbitals required for achieving p-type dopability.

Table 1. Calculated bandgaps (in eV) with various functionals as well as experimental bandgaps or other associated physical properties for TeO_2 polymorphs.

Polymorph	Experimental	PBE	$HSE^{0.25}$	$HSE^{0.10}$
α-TeO_2	3.48 [29]	2.79	3.89	3.21
β-TeO_2	Yellow [25,26]	2.22	3.30	2.63
γ-TeO_2	3.41 [30]	3.06	4.21	3.51
Rutile-type TeO_2	Metallic [33]	−0.04	0.64	0.20
β-TeO_2 monolayer		2.67	3.79	3.10

For the hypothetical r-TeO_2, the band structure calculated with the $HSE^{0.10}$ is shown in Fig. 1(e). The structure reveals an indirect bandgap of only 0.20 eV, which may explain the metallic behavior of recently-reported r-TeO_2 thin films on the FeTe surface.[33] The VBM consists of antibonding states of O $2p$ and Te $5s$ orbitals, while the conduction band minimum (CBM) is predominantly derived from Te $5p$ orbitals. Despite the substantial energy difference between Te $5s$ and O $2p$ orbitals (see supplementary Table S1), the high symmetry of r-TeO_2 results in a significant coupling between these orbitals, resulting in a notably elevated VBM. Moreover, the high symmetry permits excellent dispersion of the conduction band derived from Te $5p$ orbitals. As r-TeO_2 distorts into α-TeO_2, shown in Fig. 1(f), the coupling between Te $5s$ and O $2p$ orbitals weakens dramatically, leading the VBM to be primarily composed of O $2p$ orbitals with minor contribution from the Te $5s$ states. The structural distortion also narrows the conduction band derived from Te $5p$ orbitals, widening the calculated bandgap of α-TeO_2 to 3.21 eV, which align with its transparency. For the high-pressure orthorhombic γ-TeO_2 [Fig. 1(g)], its band structure is similar to that of tetragonal α-TeO_2, but with a slightly larger bandgap, likely attributed to further symmetry reduction and bond breaking from α- to γ-TeO_2. In contrast, β-TeO_2 [Fig. 1(h)] exhibits a markedly different band structure: (i) It has a direct bandgap at the Γ point, unlike the indirect bandgaps of α-TeO_2 and γ-TeO_2; (ii) The bandgap of β-TeO_2 is 2.63 eV, significant smaller than those of α- and γ-TeO_2, correlating with its coloration; (iii) The band edges of β-TeO_2 exhibit high anisotropy, with pronounced dispersion along the Γ-Y and Γ-X directions and localized behavior along the Γ-Z direction, reflecting its layered structure.

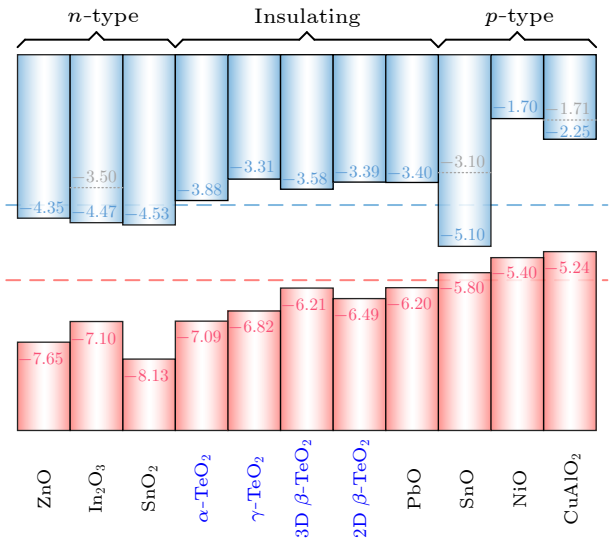

Fig. 2. Band alignment of TeO_2 polymorphs and related oxides. The energies are with respect to the E_{vac}. The data for the TeO_2 polymorphs is theoretical, while the data for other compounds is experimental (listed in supplementary Table S2). Empirically, semiconductors with CBM deeper than the blue dashed line (−4 eV) can be doped n-type, while semiconductors with VBM shallower than the red dashed line (−6 eV) can be doped p-type. Notably, for the TeO_2 polymorphs, the CBMs are shallower than the empirical CBM threshold of −4.0 eV, while the VBMs are deeper than the empirical VBM threshold of −6.0 eV, suggesting challenges in doping electrons and holes, respectively.

Base on the "doping limit rule",[34,35] the dopability of a semiconductor can be efficiently assessed by the positions of its CBM and VBM (with respect the E_{vac}). Generally, a semiconductor is more easily doped with electrons if its CBM is lower (indicating a lager electron affinity), and more readily doped with holes if its VBM is higher (indicating a smaller ionization potential). The empirical doping limit rule states that the CBM of semiconductors that can be doped with electrons is deeper than approximately −4.0 eV, while the VBM of semiconductors that can be doped with holes is shallower than approximately −6.0 eV.[5] As shown in Fig. 2, typical n-type TOSs such as ZnO,[36] In_2O_3,[37] and SnO_2[38] have CBMs deeper than −4.0 eV, while common p-type TOSs like SnO,[10] NiO,[39] and $CuAlO_2$[40] exhibit VBMs shallower than −6.0 eV. These empirical observations have provided guidance in the exploration of TOSs, particularly p-type ones. For instance, PbO (a homolog of p-type SnO) was expected to be a p-type TOS but proved challenging to dope as its VBM (−6.2 eV) surpasses the empirical VBM threshold.[11] This is because the Pb 6s orbital is much deeper in energy compared to the Sn 5s orbital due to the relativistic effect,[7] limiting the ability to elevate the VBM. To evaluate the dopability of the well-recognized α-, β-, and γ-TeO_2 polymorphs, we calculated their band edge positions, as summarized in Fig. 2. Obviously, the α-, β-, and γ-TeO_2 polymorphs exhibit CBMs and VBMs that exceed empirical thresholds, suggesting challenges in doping with electrons and holes. Specifically, the VBMs of synthetic colorless α- and γ-TeO_2 are −7.09 eV and −6.82 eV, respectively, significantly deeper than that of PbO, due to the deeper Te 5s orbital compared to Pb 6s orbital. β-TeO_2 exhibits a VBM of −6.21 eV, which is shallower than those of α- and γ-TeO_2 but still exceeds the empirical threshold. Notably, the 2D β-TeO_2 monolayer exhibits a deeper VBM and a shallower CBM compared to the 3D bulk, resulting in a larger bandgap due to typical low-dimensional confinement effect.

The dopability of TeO_2 can also be elucidated by examining the thermodynamics of its intrinsic defects. Similar to PbO,[11] all intrinsic defects in β-TeO_2 exhibit deep transition levels [Fig. 3(a)], signifying the absence of effective donors and acceptors. Specifically, the two distinct oxygen vacancies (V_{O1} and V_{O2}) show (+2/0) transitions at 1.69 eV and 1.42 eV below the CBM, respectively, indicating they exist in neutral states when E_F is close to CBM. On the other hand, the calculated (0/−2) transition of Te vacancy (V_{Te}) is at 0.36 eV above the VBM. This deep transition is explained by the insufficient contribution of Te $5s^2$ orbital to the VBM. Notably, the V_{Te} is a negative-U system, exhibits a (+2/−2) transition at 0.38 eV above the VBM, so the V_{Te} acts not as an acceptor but rather as a hole trap when the E_F is in the p-type region. The Te interstitial (Te_i) possesses a (0/+2) transition at 0.67 eV below the CBM, while the oxygen interstitial (O_i) shows a (0/−2) transition at 1.50 eV above the VBM, indicating that they are ineffective as donors and acceptors, respectively. The three antisite defects (denoted as Te_{O1}, Te_{O2}, and O_{Te}) can be considered as complexes involving the corresponding vacancies and interstitials, and as such, they also exhibit deep transition levels. Compared to 3D β-TeO_2, the intrinsic defects in 2D β-TeO_2 essentially shows similar deep transition levels [Fig. 2(b)].

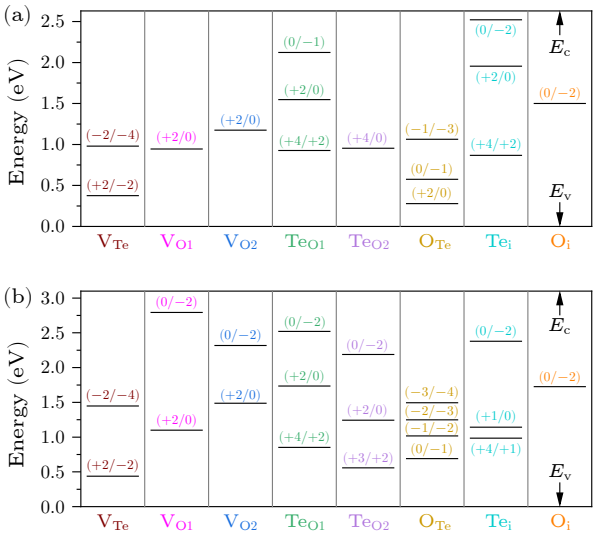

Fig. 3. Calculated defect transition levels of (a) 3D β-TeO_2 bulk and (b) 2D β-TeO_2 monolayer. "E_v" and "E_c" represent the VBM and the CBM, respectively. All intrinsic defects in both 3D and 2D β-TeO_2 exhibit deep transition levels.

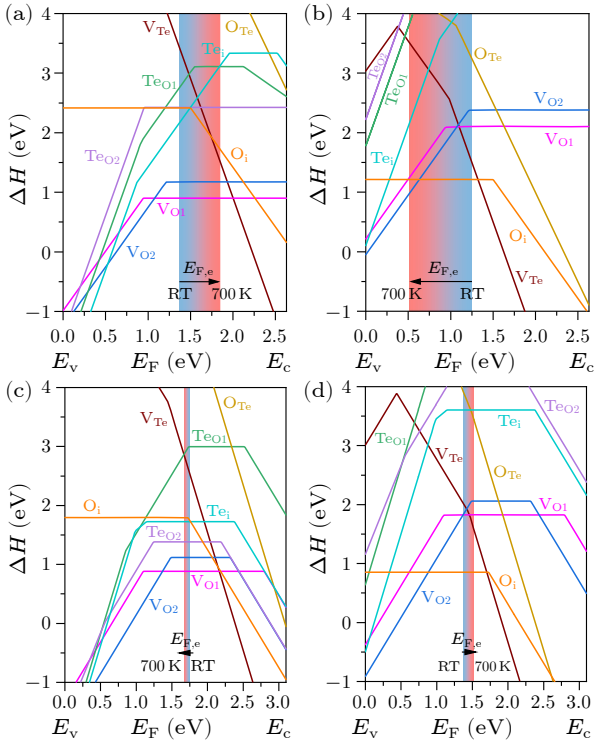

Fig. 4. Calculated formation energies (ΔH) of intrinsic defects as a function of the Fermi level (E_F) for [(a), (b)] 3D β-TeO_2 and [(c), (d)] 2D β-TeO_2 [(c), (d)] under [(a), (c)] Te-rich and [(b), (d)] O-rich conditions. The colored bars represent the ranges of equilibrium E_F ($E_{\mathrm{F,e}}$) solved with growth temperatures (T_G) ranging from room temperature to a sufficient high temperature of 700 K. Notably, for both 3D and 2D β-TeO_2, the $E_{\mathrm{F,e}}$ is situated at mid-gap, irrespective of the chemical potential and T_G, indicating constant insulating electrical properties.

Figure 4 presents the calculated defect formation energies (ΔH) of both 3D and 2D β-TeO_2. Notably, all intrinsic defects exhibit relatively high formation energies, approaching or exceeding 1 eV at equilibrium. For 3D β-TeO_2, under Te-rich/O-poor condition [Fig. 4(a)], determined by the phase equilibrium between β-TeO_2 and elemental Te, V_{O1} and V_{O2} exhibit relatively low ΔH values, making them the dominant defects, while other defects (especially V_{Te}, O_i, and O_{Te}) have significantly higher ΔH values, making their formation less feasible. However, both V_{O1} and V_{O2} primarily exist in neutral states within the mid-bandgap region. The ΔH values of doubly charged V_{O1}^{2+} and V_{O2}^{2+} are too high to release electrons effectively. Consequently, the equilibrium E_F ($E_{\mathrm{F,e}}$) of β-TeO_2 grown at room temperature (300 K) lies at the mid-gap and the corresponding electron and hole densities (n_0 and p_0) are less than $1\,\mathrm{cm}^{-3}$ (see supplementary Table S3), indicating insulating characteristics. Increasing the growth temperature (T_G) to 830 K can raise n_0 to $8.2\times10^{5}\,\mathrm{cm}^{-3}$, still insufficient to make TeO_2 a n-type semiconductor (cf. $n_0 > 10^{13}\,\mathrm{cm}^{-3}$). Conversely, under O-rich/Te-poor condition [Fig. 4(b)], determined by the phase equilibrium between β-TeO_2 and Te_2O_5, V_{Te} and O_i exhibit relatively lower ΔH values, while the others have sufficiently high ΔH values and can hardly form. In this case, O_i is stabilized in the neutral state within the mid-gap region, and the ΔH value of quadruply charged V_{Te}^{4-} is insufficiently low. Consequently, the $E_{\mathrm{F,e}}$ of β-TeO_2 grown at 300 K remains in the mid-gap region, corresponding to n_0 and p_0 values of less than $1\,\mathrm{cm}^{-3}$ and thus exhibits insulating characteristics. Raising T_G to 700 K shifts the $E_{\mathrm{F,e}}$ to 0.50 eV above the VBM and increases the p_0 to $3.1\times10^{10}\,\mathrm{cm}^{-3}$, which is still insufficient for a p-type semiconductor. These results indicate that β-TeO_2 remains electrically insulating irrespective of the synthetic chemical conditions, consistent with its excessively shallow CBM and too deep VBM.

For 2D β-TeO_2, under the Te-rich/O-poor condition [Fig. 4(c)], V_{O1} and V_{O2} exhibit relatively low ΔH values but are stabilized in their neutral states. The doubly charged V_{O1}^{2+} and V_{O2}^{2+} do not have sufficiently low ΔH values to shift the $E_{\mathrm{F,e}}$ towards the n-type region. Consequently, the $E_{\mathrm{F,e}}$ of 2D β-TeO_2 monolayer grown at 300 K is at the mid-gap. Although raising T_G increases the defect densities, $E_{\mathrm{F,e}}$ remains pinned at the mid-gap region by the deep donors and acceptors, irrespective of the T_G. Under O-rich/Te-poor condition [Fig. 4(d)], V_{Te} and O_i exhibit relatively lower ΔH values. However, doubly charged O_i^{2-} and quadruply charged V_{Te}^{4-} do not have sufficiently low ΔH values to shift the $E_{\mathrm{F,e}}$ from the mid-gap region to the p-type region. Consequently, the $E_{\mathrm{F,e}}$ of 2D β-TeO_2 monolayer grown at 300 K remains at the mid-gap. Even with increased T_G the $E_{\mathrm{F,e}}$ is pinned at the mid-gap region by the deep donors and acceptors. Therefore, like the 3D β-TeO_2 bulk, the 2D β-TeO_2 monolayer also exhibits insulating characteristics under various synthetic chemical conditions. Notably, regardless of the chemical potential condition, positively charged V_O^{2+} and Te_i^{4+} have negative ΔH values in the p-type region, while negatively charged V_{Te}^{4-} and O_i^{2-} have negative ΔH values in the n-type region. The spontaneous formation of these defects hinders the $E_{\mathrm{F,e}}$ from reaching either the p-type or n-type regions, making it impossible for the 2D β-TeO_2 monolayer to function as a TOS.

In summary, our theoretical study of the electronic structures and the dopability of TeO_2 polymorphs reveals that TeO_2, whether in the 3D bulk forms (α-, β-, or γ-TeO_2) or in the 2D β-TeO_2 nanosheets, inherently behaves as a wide-bandgap insulator. It faces significant challenges in doping with both electrons and holes due to its excessively shallow CBM and too deep VBM. The relatively deep Te $5s^2$ orbital is insufficient to raise the VBM consisting mostly O $2p$ orbitals, compared to high-lying Cu $3d^{10}$ and Sn $5s^2$ orbitals, which are more conducive to p-type dopability. For both 3D β-TeO_2 bulk and the 2D β-TeO_2 monolayer, defect calculations suggest that all intrinsic defects are deep defects with high ΔH values, causing the $E_{\mathrm{F,e}}$ to remain in the mid-gap region, independent of synthesis conditions. These findings shed light on the insulating electrical properties and doping difficulty of TeO_2, further strongly supporting our speculation that the observed p-type conductivity in the 2D β-TeO_2 samples by Zavabeti *et al.* likely stems from residual elemental Se,

reduced elemental Te, or even $Te_{1-x}Se_x$ alloy, all of which function as high-mobility p-type semiconductors.

Acknowledgements. This work was supported by the National Natural Science Foundation of China (Grant Nos. 52372150, 12088101, and 11991060) and the National Key R&D Program of China (Grant No. 2022YFB4200305).

References

[1] Chopra K L, Major S, and Pandya D K 1983 *Thin Solid Films* **102** 1
[2] Granqvist C G 2007 *Sol. Energy Mater. Sol. Cells* **91** 1529
[3] Calnan S and Tiwari A N 2010 *Thin Solid Films* **518** 1839
[4] Cai X and Wei S H 2021 *Appl. Phys. Lett.* **119** 070502
[5] Hosono H 2013 *Jpn. J. Appl. Phys.* **52** 090001
[6] Kawazoe H, Yasukawa M, Hyodo H, Kurita M, Yanagi H, and Hosono H 1997 *Nature* **389** 939
[7] Walsh A, Payne D J, Egdell R G, and Watson G W 2011 *Chem. Soc. Rev.* **40** 4455
[8] Yuan L D, Deng H X, Li S S, Wei S H, and Luo J W 2018 *Phys. Rev. B* **98** 245203
[9] Xiao Z, Du K Z, Meng W, Wang J, Mitzi D B, and Yan Y 2017 *J. Am. Chem. Soc.* **139** 6054
[10] Nomura K, Kamiya T, and Hosono H 2011 *Adv. Mater.* **23** 3431
[11] Liao M, Takemoto S, Xiao Z, Toda Y, Tada T, Ueda S, Kamiya T, and Hosono H 2016 *J. Appl. Phys.* **119** 165701
[12] Zavabeti A, Aukarasereenont P, Tuohey H, Syed N, Jannat A, Elbourne A, Messalea K A, Zhang B Y, Murdoch B J, Partridge J G, Wurdack M, Creedon D L, van Embden J, Kalantar-Zadeh K, Russo S P, McConville C F, and Daeneke T 2021 *Nat. Electron.* **4** 277
[13] Keerthana and Venimadhav A 2024 *Phys. Status Solidi RRL* **18** 2300271
[14] Hodgson S N B and Weng L 2006 *J. Mater. Sci. Mater. Electron.* **17** 723
[15] Heleskivi J, Stubb T, and Suntola T 1969 *J. Appl. Phys.* **40** 2923
[16] Beyer W, Mell H, and Stuke J 1971 *Phys. Status Solidi* **45** 153
[17] Champness C H and Kipling A L 1970 *Can. J. Phys.* **48** 3038
[18] Guo S, Qu H, Zhou W, Yang S A, Ang Y S, Lu J, Zeng H, and Zhang S 2022 *Phys. Rev. Appl.* **17** 064010
[19] Shi J, Sheng Z, Zhu L, Xu X, Gao Y, Tang D, and Zhang K H L 2023 *Appl. Phys. Lett.* **122** 101901
[20] Robertson J, Zhang X, Gui Q, and Guo Y 2024 *Appl. Phys. Lett.* **124** 212101
[21] Liu A, Kim Y S, Kim M G, Reo Y, Zou T, Choi T, Bai S, Zhu H, and Noh Y Y 2024 *Nature* **629** 798
[22] Wang J, Zheng H, Kong B, Xu X, Feng Z, Zeng T, and Wang W 2024 *ACS Appl. Mater. Interfaces* **16** 58545
[23] Leciejewicz J 1961 *Z. Kristallogr.* **116** 345
[24] Worlton T G and Beyerlein R A 1975 *Phys. Rev. B* **12** 1899
[25] Ito T and Sawada H 1940 *Z. Kristallogr.* **102** 13
[26] Beyer H 1967 *Z. Kristallogr.* **124** 228
[27] Guo S, Zhu Z, Hu X, Zhou W, Song X, Zhang S, Zhang K, and Zeng H 2018 *Nanoscale* **10** 8397
[28] Perdew J P, Burke K, and Ernzerhof M 1996 *Phys. Rev. Lett.* **77** 3865
[29] Siciliano T, Tepore A, Micocci G, Genga A, Siciliano M, and Filippo E 2009 *Sensors Actuators B Chem.* **138** 207
[30] Dewan N, Sreenivas K, and Gupta V 2007 *J. Cryst. Growth* **305** 237
[31] Heyd J, Scuseria G E, and Ernzerhof M 2003 *J. Chem. Phys.* **118** 8207
[32] Heyd J, Scuseria G E, and Ernzerhof M 2006 *J. Chem. Phys.* **124** 219906
[33] Peng K, Ren W, Wu Y, Ru H, Lu S, Chen A, Wang P, Fang X, Li H, Chi L, Ding S, Wang L, Wang Y, and Li F 2022 *J. Mater. Sci.* **57** 10225
[34] Zhang S B, Wei S H, and Zunger A 1998 *J. Appl. Phys.* **83** 3192
[35] Zhang S B, Wei S H, and Zunger A 2000 *Phys. Rev. Lett.* **84** 1232
[36] Aranovich J A, Golmayo D, Fahrenbruch A L, and Bube R H 1980 *J. Appl. Phys.* **51** 4260
[37] Nazarzadehmoafi M, Machulik S, Neske F, Scherer V, Janowitz C, Galazka Z, Mulazzi M, and Manzke R 2014 *Appl. Phys. Lett.* **105** 162104
[38] Islam M N and Hakim M O 1986 *J. Mater. Sci. Lett.* **5** 63
[39] Fu G, Wen X, Xi S, Chen Z, Li W, Zhang J Y, Tadich A, Wu R, Qi D C, Du Y, Cheng J, and Zhang K H L 2019 *Chem. Mater.* **31** 419
[40] Brahimi R, Bellal B, Bessekhouad Y, Bouguelia A and Trari M 2008 *J. Cryst. Growth* **310** 4325